Evaluation of standard imaging techniques and volumetric preservation of nervous tissue in genetically identical offspring of the crayfish *Procambarus fallax* cf. *virginalis* (Marmorkrebs)

Emanuel S Nischik [1] , **Jakob Krieger** Corresp. [1]

[1] Zoological Institute and Museum, Cytology and Evolutionary Biology, Ernst-Moritz-Arndt Universität Greifswald, Greifswald, Germany

Corresponding Author: Jakob Krieger
Email address: jakob.krieger@uni-greifswald.de

In the field of comparative neuroanatomy, a meaningful interspecific comparison demands quantitative data referring to method-specific artifacts. For evaluating the potential of state-of-the-art imaging techniques in arthropod neuroanatomy, micro-computed X-ray microscopy (µCT) and two different approaches using confocal laser-scanning microscopy (cLSM) were applied to obtain volumetric data of the brain and selected neuropils in *Procambarus fallax* forma *virginalis* (Crustacea, Malacostraca, Decapoda). The marbled crayfish *P. fallax* cf. *virginalis* features a parthogenetic reproduction generating genetically identical offspring from unfertilized eggs. Therefore, the studied organism provides ideal conditions for the comparative analysis of neuroanatomical imaging techniques and the effect of preceding sample preparations of nervous tissue. We found that wet scanning of whole animals, conducted with µCT turned out to be the least disruptive method. However, in an additional experiment it was discovered that fixation in Bouin's solution, required for µCT scans, resulted in an average tissue shrinkage of 24 % compared to freshly dissected and unfixed brains. The complete sample preparation using fixation in half-strength Karnovsky’s solution of dissected brains led to an additional volume decrease of 24 %, whereas the preparation using zinc-formaldehyde as fixative resulted in a shrinkage of 19 % in comparison to the volumes obtained by µCT. By minimizing individual variability, at least for aquatic arthropods, this pioneer study aims for the inference of method-based conversion factors in the future, providing a valuable tool for reducing quantitative neuroanatomical data already published to a common denominator. However, volumetric deviations could be shown for all experimental protocols due to methodological noise and/or phenotypic plasticity among genetically identical individuals. Micro-computed X-ray microscopy using undried tissue is an appropriate non-disruptive technique for allometry of arthropod brains since spatial organ relationships are conserved and tissue shrinkage is minimized. Collecting tissue-based shrinkage factors according to specific sample

preparations might allow a better comparability of volumetric data from the literature, even if another technique was applied.

Evaluation of standard imaging techniques and volumetric preservation of nervous tissue in genetically identical offspring of the crayfish *Procambarus fallax* cf. *virginalis* (Marmorkrebs)

EMANUEL SET NISCHIK[1] AND JAKOB KRIEGER[1*]

[1] Ernst-Moritz-Arndt-Universität Greifswald, Zoological Institute and Museum, Cytology and Evolutionary Biology, Soldmannstraße 23, 17489 Greifswald

Contact: en122971@uni-greifswald.de; jakob.krieger@uni-greifswald.de

[*]corresponding author

Abstract

In the field of comparative neuroanatomy, a meaningful interspecific comparison demands quantitative data referring to method-specific artifacts. For evaluating the potential of state-of-the-art imaging techniques in arthropod neuroanatomy, micro-computed X-ray microscopy (μCT) and two different approaches using confocal laser-scanning microscopy (cLSM) were applied to obtain volumetric data of the brain and selected neuropils in *Procambarus fallax* forma *virginalis* (Crustacea, Malacostraca, Decapoda). The marbled crayfish *P. fallax* cf. *virginalis* features a parthogenetic reproduction generating genetically identical offspring from unfertilized eggs. Therefore, the studied organism provides ideal conditions for the comparative analysis of neuroanatomical imaging techniques and the effect of preceding sample preparations of nervous tissue.

We found that wet scanning of whole animals, conducted with μCT turned out to be the least disruptive method. However, in an additional experiment it was discovered that fixation in Bouin's solution, required for μCT scans, resulted in an average tissue shrinkage of 24 % compared to freshly dissected and unfixed brains. The complete sample preparation using fixation in half-strength Karnovsky's solution of dissected brains led to an additional volume decrease of 24 %, whereas the preparation using zinc-formaldehyde as fixative resulted in a shrinkage of 19 % in comparison to the volumes obtained by μCT. By minimizing individual variability, at least for aquatic arthropods, this pioneer study aims for the inference of method-based conversion factors in the future, providing a valuable tool for reducing quantitative neuroanatomical data already published to a common denominator. However, volumetric deviations could be shown for all experimental protocols due to methodological noise and/or phenotypic plasticity among genetically identical individuals.

Micro-computed X-ray microscopy using undried tissue is an appropriate non-disruptive technique for allometry of arthropod brains since spatial organ relationships are conserved and tissue shrinkage is minimized. Collecting tissue-based shrinkage factors according to specific sample preparations might allow a better comparability of volumetric data from the literature, even if another technique was applied.

Introduction

Micro-computed X-ray tomography (µCT) and three-dimensional reconstruction of internal morphological structures have opened up new possibilities for analyzing the anatomy of nervous systems in intact specimens (reviewed in Metscher, 2009; Sombke et al., 2015). In addition to vertebrates, the application of X-ray microscopy of soft tissues has been demonstrated to be useful for a variety of metazoan taxa, such as cnidarians (e.g. Holst et al., 2016), nematomorphs (Henne et al., 2016), polychaetes (e.g. Dinley et al., 2010; Faulwetter et al., 2013), mollusks (e.g. Handschuh et al., 2013), as well as arthropods (e.g. Akkari et al., 2015; Michalik et al., 2013; Sombke et al., 2015; Steinhoff et al., 2017).

Whole-mount scanning using confocal laser-scanning microscopy (cLSM) (Krieger et al., 2015; Ott & Elphick, 2003; Ott, 2008) and especially µCT are suitable methods for precisely capturing three-dimensional structures without the need of histological sections. In samples with various tissue structures densely packed together, most imaging techniques require elaborate contrasting- or staining procedures (Metscher, 2009). In most cases, the tissue must be fixed and dehydrated in advance. The fixation process ideally fulfills the function of counteracting the structural and morphological changes induced by decay, which begins immediately after death of an organism (Lang, 2013). The chosen fixative and its time of penetration, subsequent preparation and imaging technique crucially influence the preservation of the tissue's spatial morphology on which the accuracy of allometric analysis essentially depends. Ethanolic and aldehydic solutions containing formaldehyde (or its polymer paraformaldehyde) or glutaraldehyde are the most widely used chemical fixatives in histology. Aldehydic fixatives protect proteins against denaturation by cross-linking them. No fixative preserves all structures alike, thus usually mixtures are applied (e.g. Bouin or Karnovsky) to compensate adverse effects of single components. Obviously, the preparation should aim to maintain an isotonic milieu for tissue preservation (reviewed in Lang, 2013). For µCT, contrast-enhancing, especially for the visualization of soft tissues (Gignac et al., 2016; Holst et al., 2016; Metscher, 2009; Mizutani & Suzuki, 2012), is usually realized by increasing adsorption of X-rays applying solutions containing iodine (I_2), osmium tetroxide (OsO_4), or phosphotungstic acid ($H_3PW_{12}O_{40}$) as was demonstrated by Metscher (2009). The sample manipulation in preparation for tomographic imaging for both cLSM as well as µCT, generally increases the vulnerability to artifacts (Buytaert et al., 2014). Shrinkage artifacts, due to chemical treatment (Lang, 2013) or the scanning itself (Gianoncelli et al., 2015), are very common and apart from mechanical distortions

(e.g. caused by bruises and cracks), cannot be fully eliminated even with careful handling (Buytaert et al., 2014). Furthermore, artifacts induced by radiation or chemicals might be occasionally neglected or greatly underestimated in comparative scientific reviews, which might lead to erroneous interpretations.

Since more than one hundred years, neuroanatomists always aspired to make their findings quantifiable by inventing more and more ingenious morphometric and allometric methods (see e.g. Hanström, 1926; Snell, 1891). For a meaningful interspecific comparison, quantitative data referring to method-specific artifacts could serve as rewarding tool. Increasing availability of neuroanatomical volumetric data, collected by the use of different methodological approaches of various arthropods (Beltz et al., 2003; Grabe et al., 2015; Hanström, 1926; Schmidt, 2016; Sombke et al., 2015; Tuchina et al., 2015), raises demand for standardizing these data *a posteriori*, which constitutes the emphasis of this study. For this purpose, three different well-established sample preparations including two tomographic imaging techniques (cLSM and µCT) were performed on *P. fallax* cf. *virginalis*. Well identifiable and quantifiable substructures in the crayfish brain such as the deutocerebral chemosensory neuropil (DCL) and the (deutocerebral) accessory neuropil (AcN) served as approximation for volume change of tissues. The parthenogenetic marbled crayfish *Procambarus fallax* forma *virginalis* (Martin et al., 2010) provides for a rewarding model organism (review: Harzsch et al., 2015) featuring a textbook example of a “typical” astacid brain. The uncomplicated husbandry and year-round parthenogenetic reproduction of the marbled crayfish enables replicable tests using high sample numbers (review: Vogt, 2011).

Materials and Methods

Nomenclature

The neuroanatomical nomenclature used in this manuscript is based on Sandeman et al. (1992) and Richter et al. (2010) with some modifications adopted from Harzsch & Hansson (2008), Kenning and Harzsch (2013), and Loesel et al. (2013). The term “oesophageal connective” and the corresponding abbreviation OC (British English) are maintained here for simplicity. The

114 syncerebral brain mass excluding the lateral protocerebrum and visual neuropils of the eyestalks
115 (see Krieger et al., 2015) is termed “central brain” throughout the text according to Schmidt
116 (2016). Although, sample preparations as well as imaging techniques according to the three
117 protocols used vary in a vast of parameters that influence the resulting volume data, each of the
118 three fixatives (zinc-formaldehyde fixative, Bouin’s as well as half-strength Karnovsky’s
119 solution) is used as a synonym for the entire protocol throughout the text.

120

121 **Animals**

122 The specimens of *P. fallax* cf. *virginalis* used in our study were obtained from a commercial
123 aquarium shop (Aquaristik-Langer GbR, https://aquaristik-langer.de/) and were kept together in a
124 freshwater tank at the facilities of the University of Greifswald. For the experimental design,
125 berried individuals were isolated from a community tank, to ensure that all larvae originated
126 from a single individual, and hence were genetically identical. A total of 24 individuals were
127 harvested for pre-tests directly after the juveniles left the maternal pleopods. At this
128 developmental stage, the average body length (rostrum to pleon) measured about 5 mm and the
129 juveniles started autonomous feeding. Morphometric measurements were performed on dead and
130 undissected juveniles in order to ensure that individuals were of the same size. Morphometric
131 analysis was conducted using a Nikon eclipse 90i microscope connected to a Nikon camera DS2-
132 MBWc. For each specimen carapace length and eyestalk width were measured by using the
133 software NIS-Elements AR 3.0. Application of the Shapiro-Wilk-test using the statistical
134 software R 3.2.3 showed normal distribution for carapace length ($p = 0.8688$) and eyestalk width
135 ($p = 0.3054$) among the samples. Subsequently, Welch’s Two Sample t-test assured that there
136 was no significant difference in measured morphological characters between samples used for
137 cLSM and µCT analysis (carapace length, $p = 0.1925$; eyestalk width, $p = 0.1034$). Furthermore,
138 several adult animals were kindly provided by Gerhard Scholtz (Humboldt University, Berlin,
139 Germany) and were kept as described above.

140

141 **General sample preparation**

Genetically identical juveniles of *Procambarus fallax* cf. *virginalis* from the same hatch were taken out of separate tanks with plastic pipettes. They were anaesthetized by chilling them at -18 °C in a beaker with little water for a few minutes. Then, the anaesthetized animals were killed by transferring them into watch glasses containing 4 % paraformaldehyde (PFA) and phosphate buffered saline (PBS, pH 7.4; 0.1 M) for 30 minutes at room temperature on the shaker. After that, PFA was removed by immersing the dead specimens in fresh PBS (for fixation in half-strength Karnovsky's as well as Boiun's solution) or HEPES (for fixation in ZnFA) on the shaker for two times (5 min each) at room temperature before fixation or brain dissection took place.

Sample preparation for µCT

Before µCT-scanning, seven juvenile siblings were transferred into Eppendorf tubes and immersed in Bouin's solution (10 % formaldehyde, 5 % glacial acetic acid in saturated aqueous picrinic acid). Fixation took place for one week in a fridge (4 °C). After fixation, the animals were gradually dehydrated in ethanol at room temperature (30 %, 50 %, 60 %, 70 %, 80 %, 90 %, 96 %, and 3 x in 99.5 % ethanol) for 30 min for each step. For enhancing the contrast, samples were incubated in iodine solution (2 % iodine resublimated [Carl Roth GmbH 1 Co. KG, Karlsruhe, Germany; cat. #X864.1] in 99.5 % ethanol) for 24 h in the fridge. Iodine was subsequently washed out of the samples for 5 × 3 min with ethanol. Wet specimens were scanned in a glue sealed pipette tip filled with 99.5 % ethanol (according to Sombke et al., 2015).

µCT-Scanning

The scans were performed with a laboratory scaled X-ray-microscope (Xradia MicroXCT-200; Carl Zeiss Microscopy GmbH) entailing geometric and optical magnification. The Bouin-fixed samples of *P. fallax* cf. *virginalis* were scanned with a 20× objective in 99.5 % ethanol with a voltage of 40 kV, a current of 200 µA, and an exposure time of 8 seconds. For all scans, binning 2 was applied (summarizing 4 pixels for noise reduction). Projections obtained by the tomography were reconstructed using the software XMReconstructor (Carl Zeiss Microscopy

GmbH). To avoid consequent information loss, binning 1 (full resolution) was applied for the following reconstruction resulting in image stacks of 993 × 993 pixels and a pixel size of about 1.1 µm.

For the inference of an individual *in vivo* volume during µCT sample preparation and the comparison of chemically-induced effects on the brain volume, brains were dissected, under tap water at RT from a total of another six adult animals of different sizes, and each was immediately scanned (stage 1) moistly within a sealed Eppendorf tube at 20 kV and 3 W for 1 sec (binning 4) with 400 projections reducing the total scan time to 15 min. Brains were subsequently fixed in Bouin's solution overnight in the fridge. Bouin's solution was replaced two times by tap water and the brain was immediately scanned (stage 2) again moistly using the identic scanning parameters. Afterwards, brains were gradually dehydrated as outlined above in addition with contrast enhancement by dissolved iodine (2 %) in ethanol before being scanned a third time (stage 3) in 99.5 % ethanol using again the same scanning parameters.

Sample preparation for cLSM

Fixation in half-strength Karnovsky's solution for enhancing autofluorescence of nervous tissue

The two pairs of antennae as well as the eyestalks were removed and the brains of a total of six specimens were dissected in phosphate buffered saline (PBS; 0.1 M; pH 7.4) using precision forceps (DUMONT®; type 55). The brains were fixed in half-strength Karnovsky's fixative, a mixture of 2 % glutaraldehyde [Electron Microscopy Sciences, 1560 Industry Road, USA-Hatfield, PA 19440; Cat-No. 16220] and 2 % PFA [Carl Roth GmbH 1 Co. KG, Karlsruhe, Germany; Cat-no. 0335.2] in PBS (0.1 M; pH 7.4) for a week at 4 °C. Subsequently, a gradual dehydration of the samples was conducted in ethanol (50 %, 70 %, 80 %, 90 % for 10 min each, 96 % for 30 min, and in 99.5 % ethanol for 2 x 30 min) at room temperature.

Fixation in zinc-formaldehyde and immunhistochemical labeling

The whole mount labeling protocol after Ott (2008) was applied to improve antibody penetration into nervous tissues, as compared to traditional PFA-fixation. For this method, a total of seven animals were killed by a few drops of formalin instead of 4 % PFA in PBS to avoid precipitation of zinc phosphate in combination with zinc-formaldehyde in the following steps (compare Ott, 2008). The central brain was then dissected in HEPES-buffered saline (HBS) as described before and fixed in 4 % zinc-formaldehyde (ZnFA; Electron Microscopy Sciences, 1560 Industry Road, USA-Hatfield, PA 19440; Cat-No. 15675) on a shaker for 20 h at room temperature. The fixed brains were subsequently washed for 3 x 15 min in HBS, and instantly dehydrated and postfixed in DENT's fixative (20 % DMSO [Serva Electrophoresis, Heidelberg, Germany; Cat-No. 20385] / 80 % methanol) in a drop of HBS on the shaker again for 2 h, at room temperature. Afterwards, the brains were transferred into 99 % methanol. The samples were gradually rehydrated in TRIS-buffer with varying grades of methanol (90 %, 70 %, 50 %, 30 % methanol, and finally, pure TRIS-buffer for 15 min each). Samples were preincubated for 2 x 2 h in PBS-TX (0.3 % triton, 0.02 % sodium azide, 1 % bovine serumalbumin [BSA]) at room temperature, followed by incubation in monoclonal mouse anti-synapsin antibody (3C11 anti SYNORF1; Developmental Studies Hybridoma Bank, University of Iowa; deposited by E. Buchner, University Hospital Würzburg, Germany; diluted 1:1 in glycerol) in PBS (1:1000) for 4 days at 4 °C. Excess primary antibody was washed in PBS-TX for 4 x 30 min at room temperature. Incubation of the Cy 3-conjugated secondary antibody (goat anti-mouse; Jackson Immuno Research; 1:1 in glycerol) in HBS (1:500) was carried out in the fridge (4 °C) for 2.5 days. After washing for 2 x 1 h in PBS-TX, the samples were dehydrated in ethanolic solutions of different grades (30 %, 50 %, 70 %, 80 %, 90 %, 96 %, and 99.5 % for 30 min each) at room temperature. Regarding antibody specificity, has been shown that the monoclonal mouse-anti-*Drosophila* antibody 3C11 consistently labels synaptic brain regions in representatives of all major subgroups of the malacostracan crustaceans (see Beltz et al., 2003; Harzsch & Hansson, 2008; Harzsch et al., 1997, 1999, Krieger et al., 2012, 2015; Meth et al., 2017; Vilpoux et al., 2006). Hence, it can be assumed that this antibody does in fact label synaptic neuropils in Malacostraca (for more details see Krieger et al., 2015).

cLSM-scanning

Scanning was conducted on a confocal laser-scanning microscope (Leica TCS SP5 II). For optimal light transmission, tissues were cleared in 98 % methyl salicylate (Merck, Darmstadt, Germany; Cat-no. W274518). After dehydration in ethanol, brains that were previously fixed in ZnFA (n=7) as well as in half-strength Karnovsky's solution (n=6) were transferred into custom-made scan chambers filled with pure methyl salicylate before confocal laser-scanning. Scanning was performed with an inverted Leica TCS SP5II (Leica, Wetzlar, Germany) using a DPSS-laser with an excitation wavelength of 561 nm and a speed of 400 Hz. For detection of fluorescence (emitted by glutaraldehyde-enhanced autofluorescence as well as by Cy3-conjugates of the secondary antibody), a 10 x objective with a numerical aperture of 0.4 was used resulting in stacked images of 1024 x 1024 pixels with a pixel size of about 0.8 µm. The confocal microscope operated with a pinhole size of 53 µm in diameter and in steps of 1.33 µm (system-optimized to 1 airy unit).

Data processing

Volume reconstruction and visualization was carried out using Amira 5.6.0. (FEI Visualization Science Group, Burlington, USA). The central brain, the deutocerebral chemosensory lobes (DCLs) as well as the accessory lobes (AcNs) were segmented manually for volumetric analysis. Three-dimensional surfaces corresponding to the segmentation were generated using unconstrained smoothing (Amira: SurfaceGen). Voxel data of the reconstructed neuropils were extracted by using Amira`s material statistics tool. The outline of scans of dissected brains could be instantly visualized without further virtual segmentation by using the Amira Isosurface-module. Morphological deformations based on anisometric shrinkages could be detected this way.

Raw data of brain section series (based on µCT as well as cLSM) is available from https://www.morphdbase.de (Grobe & Vogt, 2009) under the "media" tab under "Krieger". A combination of the short title "Nischik and Krieger (2017) Marmorkrebs", an identifier according to the specimen, and an abbreviation for the method applied (e.g. Nischik and Krieger (2017) Marmorkrebs01_µCT) is given for each of the 20 image stacks in addition to 18 image stacks of brains of another six adult specimens which were scanned 1) freshly dissected prior to

fixation; 2) fixed with Bouin's solution overnight but without any dehydration as well as any contrast agent; and 3) after fixation, dehydration in ethanol, and contrast enhancement using 2% iodine.

Furthermore, additional table S1 summarizes the volumes of the central brain, of the DCLs, and AcNs of both brain hemispheres according to the three methods applied as well as the z-corrected volumes due to a putative refractive mismatch in cLSM-scans. In additional table S2, the volumes of the central brain of six adult specimens are summarized which were analyzed for evaluation of tissue shrinkage throughout the sample preparation (stages 1 to 3) prior to µCT-scanning of fixed and contrast-enhanced samples.

Statistics

The acquired volume data (Fig. 1) were exported into Microsoft® Excel for descriptive statistics. Statistical analyses were performed with the "stats"-package and illustrated with the "graphics"-package of R 3.2.3. A one-way analysis of variance (ANOVA) was carried out for calculation of statistical significant differences between volumetric data and the methods used (Fig. 2). The effects of treatment on the volume of the subunits DCLs and AcNs, as well as on the total volume of the central brain were calculated for each structure by Tukey's post-hoc test. A paired two sample Student's t-test was applied for volumes of left and right lobe of AcN and DCL respectively, to test reproducibility of the manual volume reconstruction, which was conducted by the same investigator for each specimen. A Wilcoxon signed rank test was applied to test the effect of chemically induced difference in the brain volume throughout the sample preparation for µCT-scanning.

Results

µCT

Tomograms were generated with µCT to morphometrically analyze the brain of *P. fallax* cf. *virginalis*. Volume rendering allowed virtually sectioning of the animal in different planes for

neuroanatomical analysis as well as visualizing the brain in its natural position within the cephalon (Figs. 3A to D). The image contrast as a function of the tissue density was high enough to allow identification of single neuropils (compare Figs. 4A and B). Thus, the central brain including deutocerebral chemosensory lobes (DCLs) and accessory neuropils (AcNs) could be reconstructed (Figs. 3C and D). The central brain is vertically curved and held in its upright position by the protocerebral tract originating in the lateral protocerebrum (latPC; Figs. 3C and D) within the eyestalks as well as by the nerves of the antennae 1 and 2 (A_I and A_{II}; Figs. 3A and C). Here, an approximate *in situ* coherent reconstruction of the neuropils in their spatial context is assumed, since only a few steps of sample preparation were required for scanning an animal as a whole.

While µCT-scanning of contrasted tissues delivered a high image contrast, the analysis of µCT-scans of unfixed as well as fixed brains (without any contrast agent) of another six adult specimens, which were used for inferring individual *in vivo* volumes during µCT sample preparation, turned out to be fairly challenging. In freshly dissected as well as in Bouin-fixed but uncontrasted brains, the image contrast was barely high enough to identify the limits of the tissue surfaces but did not suffice to identify internal substructures such as neuropils or cell clusters. The central brain volume resulted in a significantly average shrinkage of 24 % (ranging from 7.9 to 44.8 %) after fixation in Bouin's solution (Wilcoxon signed rank test: $p = 0.0313$; $n = 6$) and no further significant shrinkage (Wilcoxon signed rank test: $p = 0.6875$; $n = 6$) after dehydration and contrast-enhancement using 2 % iodine in ethanol (Fig. 5 and table S2).

cLSM

Autofluorescence in half-strength **Karnovsky's solution**

Tissues fixed with half-strength Karnovsky's solution resulted in cLSM scans characterized by a high resolution and remarkable signal to noise ratio. Furthermore, intricate histological details such as individual olfactory glomeruli in the DCL and even microglomeruli within the AcN were resolved with high accuracy (compare Figs. 4A and C).

Immunhistochemistry, ZnFA-Fixation

In comparison to the previously described method, volume divergences may only be the result of the fixation of the specimen – in this case using the ZnFA-fixation protocol after Ott (2008) and, of course, of the individual bias, due to manual segmentation for three-dimensional reconstruction in Amira. In fact, the reconstructed volumes differ only slightly, and thus, no statistically significant difference between the applied fixations (ZnFA and half-strength Karnovsky's solution) could be detected for each of the brain substructures analyzed (Fig. 2). However, a slightly higher average volume indicates, that the whole brain is somewhat better preserved by using the fixation with ZnFA and dehydrogenation in methanol and DMSO. Since an immunohistochemical labeling was used here, the resulting tissue contrast is different to that of autofluorescence in half-strength Karnovsky's solution(compare Figs. 4C and D). In this case, primarily areas in which the synaptic membrane protein synapsin was present were stained (Fig. 4D). While the intention was to facilitate the identification of neuropil regions, it actually increased image noise.

µCT *versus* cLSM

All three methods very likely differ to a certain degree from *in vivo* congruent nervous tissue volume. Since all samples at least temporarily were exposed to hyperosmolar media resulting in dehydration, it has to be assumed that artifacts due to shrinkage most likely occurred. An expansion of the tissue seems unlikely, since also in the wet-scan µCT approach, dehydration takes place (e.g. fixation in Bouin's solution, dehydration in ethanol). A significant difference between the volumes of nervous tissue (DCL) could be ascribed to thevc general imaging technique (µCT *vs*. cLSM: Welch's Two Sample t-test: $p = 0.0013$; $n = 20$), whereas the choice of fixative between both cLSM approaches did not influence the tissue volume significantly (Welch's Two Sample t-test: $p = 0.4541$; $n = 13$). Assuming a symmetrical development of both brain hemispheres, the investigator's individual bias in manual segmentation for three-dimensional reconstruction was tested by comparing volumes of both hemispheres. While the volume of the accessory lobes reliably exceeded the volume of the deutocerebral chemosensory lobes (single-factor ANOVA: $p < 0.001$; $n = 20$), no difference in the volume of the left and right hemispheres of paired lobes could be found in any given treatment (paired Student's t-test: DCL: $p = 0.2691$; AcN: $p = 0.1107$; $n = 20$).

The highest DCLs-volumes (total volume of both hemispheres) were reconstructed in specimens which were fixed in Bouin's solution and imaged by the use of µCT (mean DCLs volume [mm^3]: 0.0029 ± 0.0003; n = 7). The DCLs volumes in specimens fixed in ZnFA (mean DCLs volume [mm^3]: 0.0023 ± 0.0006; n = 7) were insignificantly higher compared to specimens fixed in half-strength Karnovsky's solution (mean DCLs volume [mm^3]: 0.0021 ± 0.0003; n = 6). The measured volume of nervous tissue was most congruent to assumed *in vivo* volume when specimens were fixed in Bouin and scanned in ethanol with µCT (Figs 1, 2, and 5). This is followed by cLSM visualization of whole-mounts fixed in ZnFA and at last of tissues fixed in half-strength Karnovsky's solution (compare Figs. 1A, B, and C). Although µCT derived volumes are significantly smaller than those of freshly dissected brains (average of 24 %, ranging from 7.9 to 44.8 %), cLSM tomograms of tissues fixed in half-strength Karnovsky's solution reveal a further relative shrinkage of 24 %; and of 19 % when using ZnFA-fixation.

In *P. fallax* cf. *virginalis*, light-microscopic imaging techniques on the brain require the removal of the cuticle or dissection of the nervous tissue, thus an analysis of the brain within the animal is only feasible by using x-ray -or magnetic resonance imaging techniques (Brinkley et al., 2005; Herberholz et al., 2004; Köhnk et al., 2017, and reviewed in Ziegler et al., 2011). Three-dimensional surfaces of half-strength Karnovsky's solution-fixed brains, based on isosurfaces using a grayscale-threshold (Amira: Isosurface), appeared more porous and wrinkled (compare Figs. 6A to C), while the ZnFA-fixed brains had a smoother appearance (compare Figs. 6D to F). Along the neuraxis, brains appear more furrowed after fixation with half-strength Karnovsky's solution compared to those fixed with ZnFA (Figure 6). In addition, the bilaterally symmetric antenna-2-nerve ($A_{II}Nv$; Figs. 6D and F) was better preserved in its fibrous organization in ZnFA preparations compared to those fixed with half-strength Karnovsky's solution (Figs. 6A and C). For comparison of image quality, a schematic overview of the central brain (Fig. 4A) as well as virtual frontal sections recorded on a similar anatomical plane (approximately as shown in Fig. 3B) are shown in Figure 4B to D. In images generated by cLSM within the DCL, individual olfactory glomeruli are visible (Figs. 4C and D). The images produced by µCT have a lower resolution and a lower signal-to-noise ratio. Here, the identification of individual olfactory glomeruli at least at the chosen magnification is not possible (Figure 4B). In fact, the highest contrast was obtained by confocal imaging of half-strength Karnovsky's solution-fixed tissue

(Fig. 4C). By the use of autofluorescent enhancement of half-strength Karnovsky's solution-fixation, the sample preparation is much less time consuming but more unspecific than applying the two-step protocol of immunhistochemical labeling. The high resolution in both methods reveals details like individual olfactory glomeruli of the DCLs as well as even microglomeruli within the AcNs (Figs. 4A, C, and D).

Discussion

Confocal laser-scanning microscopy turned out to be the most suitable technique for identification of neuropils and neuronal somata (Figs. 4A, C, and D). Nevertheless, for the use of brain morphometry at a coarse level, the image contrast is sufficient to distinguish the neuropils from the surrounding tissue in all applied techniques. In contrast to the preparation for µCT, the central brain has to be dissected for cLSM whole mounts, which comes with some disadvantages. The process of sample preparation alters the brain's characteristic shape, which *in-situ* is displaying a curvature along the neuraxis. Due to dissection, the originally upstanding central brain collapses so that spatial relationships of brain regions become artificial. In addition, the use of methyl salicylate for clearing in advance of cLSM-scanning has been reported to cause shrinkage of nervous tissues ranging from 3.5 to 27 % of the volume (Bucher et al., 2000). Furthermore, a possible refractive mismatch along the z-axis must be taken into account for the use of methyl salicylate as mounting medium for cLSM which can lead to enormous aberrations of volume (Bucher et al., 2000). However, using the correction factor for the refractive mismatch for the use of methyl salicylate provided by Bucher et al. (2010) of 1.581 (for a 10x dry objective with a numerical aperture of 0.40) resulted in a drawn-out appearance of the brains and led to an aberrant ratio between the dimensions in xy-axis and z-axis. By manually adjusting the voxel z-dimension of confocal image stacks by a factor of 1.188, led to spatial congruence of the brain dimensions of µCT-scans. The resulting volumes of brains fixed in ZnFA as well as in half-strength Karnovsky's solution were still insignificantly smaller (ZnFA *vs.* Bouin: 5 %; $p = 0.826$; half-strength Karnovsky's solution *vs.* Bouin: 12.5 %; $p = 0.362$; one-way ANOVA) than those obtained from µCT-scans. Although, brain volumes based on cLSM-stacks that were axially rescaled are insignificantly smaller, the sample preparation seems to have a higher influence on tissue shrinkage than the sample preparation for µCT-scanning.

While volumetry can be helpful to analyze differences in the size relation of brain structures within an organism, as well as for interspecific comparison, referring brain size as a function of cognitive capacity, is highly debated (Chittka & Niven, 2009; Healy & Rowe, 2013). However, for example in honeybees (Durst et al., 1994; Groh et al., 2006) or in leaf-cutting ants (Groh et al., 2014), morphometric analysis showed an age and experience dependent difference in neuropil volume of the mushroom body. Especially for the volumetry of these tiny brain subcompartiments, measurement errors can have a huge impact and should therefore be minimized. It is therefore important to consider the osmolality of immersive chemicals (fixatives and buffers) in respect to the target tissue. Increased tissue shrinkage was reported with increasing hypertonia (Rasmussen, 1974), hence chemical fixatives with similar osmolality as the original osmotic environment (e.g. < 280 mOsm/kg H_2O for freshwater species) are recommended (Bullock, 1984; Coetzee & van der Merwe, 1985). An area shrinkage of 11 - 20 % was reported for rabbit corneal endothelial cells fixed with Karnovsky fixative (850 mOsM/kg; Doughty et al., 1997). However, in the current study merely a half-strength Karnovsky fixative (640 mOsM/kg; Platt et al., 1997) was applied. Ott (2008) described a new fixation protocol for immunhistochemical staining, which uses ZnFA instead of PFA resulting in lower osmolality (325 mOsm/kg). This has been shown to improve antibody penetration and preservation of spatial brain morphology. Ott (2008) demonstrated effects of different fixation protocols on morphological preservation on the brain of the desert locust *Schistocerca gregaria*. Ott showed that fixation using paraformaldehyde lead to increased wrinkling in contrast to ZnFA-fixation. Likewise, the nature of dehydration and the duration of fixation were found to be decisive factors. This corresponds to findings from Ott (2008), as preparations with a shorter fixing time in ZnFA showed a lower wrinkling. Here, the cLSM-tomograms resulted in smoother surfaces of brains analyzed.

Apart from indirect volumetric measurements evaluated here, a possible approach to obtain approximate *in vivo* volumes for invertebrate brains, would be the use of a micro-volumeter according to Douglass and Wcislo (2010), as an example for direct volumetry. By the use of Archimedes' principle, the dissected brain is put in a liquid-filled tube and the occurring volume displacement of the liquid can be measured with a micro-pipette stepwise until the previous meniscus is reached. In this way, the total removed volume equals the actual brain volume. However, based on initial trials, instrumental errors still outweigh a precise measurement of very

small volumes. This technique needs more precise adjustment for readout of the meniscus. A successful application of direct volumetry using Archimede's principle or high resolution magnetic resonance imaging of living animals will offer a conclusive reference for *in vivo* brain volumes. Although the sample size is not markedly high (n = ranging from 6 to 7 per treatment), we consider that specimens prepared for µCT feature the closest *in vivo* coherence (24 % average shrinkage; ranging from 7.9 to 44.8 %). We could show that shrinkage due to each single step throughout the sample preparation was primarily influenced by the fixation in Bouin, whereas the subsequent steps of this preparation interestingly did not contribute substantially to tissue shrinkage. However, dehydration in ethanol in addition with contrast-enhancement by iodine (Buytaert et al., 2014) as well as the scanning procedure itself (Gianoncelli et al., 2015) indeed most likely lead to a deviation from the *in vivo* volume.

The deutocerebral chemosensory and accessory lobes are convenient landmarks for a volumetric evaluation of experimental effects, due to their conspicuous structure with an almost spherical shape, they can be easily identified. Especially for the conspicuous deutocerebral chemosensory lobes, volumetric data are available for a considerable number of crustacean species (see Beltz et al., 2003; Krieger et al., 2015; Tuchina et al., 2015; and review in Schmidt, 2016). In particular, the relative volumes of these homologous brain regions vary greatly among species. For comparison, table 1 displays the volume information for the deutocerebral chemosensory lobes of selected crustacean species accompanied by the data obtained for *P. fallax* cf. *virginalis*. However, it should be noted that all individuals of *P. fallax* cf. *virginalis* analyzed were juveniles with a body length of about 5 mm. Adults of this species can reach a body length of 120 mm, and thus larger brain sizes have to be expected. Furthermore, it can be expected that methods including chemicals do not influence volumes of different brain substructures alike (such as somata or fibers). Since the main volume of the brain is dominated by neuropils as well as the fact that all three methodological approaches did not meet the requirements of a differentiated volumetric analysis, an inhomogeneous tissue shrinkage was neglected for simplicity.

For interspecific comparisons and the corresponding phylogenetic or neuroanatomical value of volumetric data, several factors have to be standardized, such as the experimental procedure including fixatives and technique of volumetry (e.g. histological sections with volumetric extrapolations based on the section thickness, or 3D-reconstruction of tomographic data).

Shrinkage factors, based on the morphometric method and fixatives used, can serve as a tool to approximate already referred volumetric data to a common denominator for a more reasonable interspecific comparison. Because of its parthenogenetic nature, *P. fallax* cf. *virginalis* is well suited generating such a reference system at least for aquatic arthropods featuring a comparable osmolality. Although the specimens analyzed were genetically identical and of the same age (clutch), individual brain sizes might vary due to phenotypic plasticity as has been shown e.g. for the marmoration pattern in siblings of the Marmorkrebs (review: Vogt, 2011), but also for brain sizes in clones of *Daphnia magna* (Macagno et al., 1973), and also in vertebrates (review: Mitchell, 2007). Consequently, comparative brain allometry in juvenile isogenetic siblings appears to be the most favorable approximation to neglect inter-individual variations.

Conclusions

Although today, neuroanatomical volumetric data are available for a variety of crustacean species, interspecific comparisons often suffer from methodological differences in volumetry. Variations in tissue volume as artefacts of experimental sample preparation, such as fixation procedures, might be incorrectly assigned to biological phenomena. While comparative brain morphometry and especially volumetry as a measure for cognitive capabilities is controversially discussed (Chittka & Niven, 2009; Healy & Rowe, 2013), it is, however, a useful tool for other fields of interest, such as the neural development (Helluy et al., 1995), neurophylogeny as well as specific evolutionary adaptations of the nervous system (Beltz et al., 2003; Krieger et al., 2015; reviewed in Schmidt, 2016). Therefore, a standardization of method-based deviations is highly recommended. Here, we aimed at a consistent methodological approach to evaluate standard imaging techniques as well as to obtain conversion factors to deduce approximate *in vivo* volumes based on the method of analysis. Well-founded conversion factors will allow for *a posteriori* standardization of determined nervous tissue volumes in malacostracans and therefore help to eliminate the aforementioned sources of error. Due to its parthenogenetic reproduction, *P. fallax* cf. *virginalis* produces genetically identical offspring making it an ideal model organism especially for methodological studies. Further comparative studies covering all standard techniques in the same manner, will offer a conclusive reference system and comparability,

irrespective of fixation protocol chosen which is indeed dependent of the imaging technique and the specific scientific question.

Acknowledgements

We cordially thank Gerhard Scholtz (Humboldt-University of Berlin) for the kind provision of animals and Caroline Viertel (University of Greifswald) for the animal husbandry in the laboratory. We like to express our gratitude to Steffen Harzsch and Marie K. Hörnig (University of Greifswald) for reading and improving the manuscript. We would like to thank both reviewers for their input, as these recommendations led us to markedly improve the manuscript.

References

Akkari N., Enghoff H., Metscher BD. 2015. A New Dimension in Documenting New Species: High-Detail Imaging for Myriapod Taxonomy and First 3D Cybertype of a New Millipede Species (Diplopoda, Julida, Julidae). *PLOS ONE* 10:e0135243. DOI: 10.1371/journal.pone.0135243.

Beltz BS., Kordas K., Lee MM., Long JB., Benton JL., Sandeman DC. 2003. Ecological, evolutionary, and functional correlates of sensilla number and glomerular density in the olfactory system of decapod crustaceans. *The Journal of Comparative Neurology* 455:260–269. DOI: 10.1002/cne.10474.

Brinkley CK., Kolodny NH., Kohler SJ., Sandeman DC., Beltz BS. 2005. Magnetic resonance imaging at 9.4 T as a tool for studying neural anatomy in non-vertebrates. *Journal of Neuroscience Methods* 146:124–132. DOI: 10.1016/j.jneumeth.2005.02.003.

Bucher D., Scholz M., Stetter M., Obermayer K., Pflüger H-J. 2000. Correction methods for three-dimensional reconstructions from confocal images: I. tissue shrinking and axial

522 scaling. *Journal of Neuroscience Methods* 100:135–143. DOI: 10.1016/S0165-
523 0270(00)00245-4.
524 Bullock GR. 1984. The current status of fixation for electron microscopy: A review. *Journal of*
525 *Microscopy* 133:1–15. DOI: 10.1111/j.1365-2818.1984.tb00458.x.
526 Buytaert J., Goyens J., De Greef D., Aerts P., Dirckx J. 2014. Volume shrinkage of bone, brain
527 and muscle tissue in sample preparation for micro-CT and light sheet fluorescence
528 microscopy (LSFM). *Microscopy and Microanalysis* 20:1208–1217. DOI:
529 10.1017/S1431927614001329.
530 Chittka L., Niven J. 2009. Are Bigger Brains Better? *Current Biology* 19:R995–R1008. DOI:
531 10.1016/j.cub.2009.08.023.
532 Coetzee J., van der Merwe CF. 1985. Effect of glutaraldehyde on the osmolarity of the buffer
533 vehicle. *Journal of Microscopy* 138:99–105. DOI: 10.1111/j.1365-2818.1985.tb02602.x.
534 Dinley J., Hawkins L., Paterson G., Ball A d., Sinclair I., Sinnett-Jones P., Lanham S. 2010.
535 Micro-computed X-ray tomography: a new non-destructive method of assessing
536 sectional, fly-through and 3D imaging of a soft-bodied marine worm. *Journal of*
537 *Microscopy* 238:123–133. DOI: 10.1111/j.1365-2818.2009.03335.x.
538 Doughty MJ., Bergmanson JPG., Blocker Y. 1997. Shrinkage and distortion of the rabbit corneal
539 endothelial cell mosaic caused by a high osmolality glutaraldehyde-formaldehyde
540 fixative compared to glutaraldehyde. *Tissue and Cell* 29:533–547. DOI: 10.1016/S0040-
541 8166(97)80054-7.
542 Douglass J., Wcislo W. 2010. An inexpensive and portable microvolumeter for rapid evaluation
543 of biological samples. *BioTechniques* 49:566–572. DOI: 10.2144/000113464.

544 Durst C., Eichmüller S., Menzel R. 1994. Development and experience lead to increased volume
545 of subcompartments of the honeybee mushroom body. *Behavioral and Neural Biology*
546 62:259–263. DOI: 10.1016/S0163-1047(05)80025-1.
547 Faulwetter S., Vasileiadou A., Kouratoras M., Dailianis T., Arvanitidis C. 2013. Micro-
548 computed tomography: Introducing new dimensions to taxonomy. *ZooKeys* 263:1–45.
549 DOI: 10.3897/zookeys.263.4261.
550 Gianoncelli A., Vaccari L., Kourousias G., Cassese D., Bedolla DE., Kenig S., Storici P.,
551 Lazzarino M., Kiskinova M. 2015. Soft X-Ray Microscopy Radiation Damage On Fixed
552 Cells Investigated With Synchrotron Radiation FTIR Microscopy. *Scientific Reports*
553 5:10250. DOI: 10.1038/srep10250.
554 Gignac PM., Kley NJ., Clarke JA., Colbert MW., Morhardt AC., Cerio D., Cost IN., Cox PG.,
555 Daza JD., Early CM., Echols MS., Henkelman RM., Herdina AN., Holliday CM., Li Z.,
556 Mahlow K., Merchant S., Müller J., Orsbon CP., Paluh DJ., Thies ML., Tsai HP., Witmer
557 LM. 2016. Diffusible iodine-based contrast-enhanced computed tomography (diceCT):
558 an emerging tool for rapid, high-resolution, 3-D imaging of metazoan soft tissues.
559 *Journal of Anatomy* 228:889–909. DOI: 10.1111/joa.12449.
560 Grabe V., Strutz A., Baschwitz A., Hansson BS., Sachse S. 2015. Digital *in vivo* 3D atlas of the
561 antennal lobe of *Drosophila melanogaster*. *Journal of Comparative Neurology* 523:530–
562 544. DOI: 10.1002/cne.23697.
563 Grobe P., Vogt L. 2009. *Morph.D.Base 2.0: A public data base for morphological data,*
564 *metadata, and phylogenetic matrices*.

565 Groh C., Ahrens D., Rössler W. 2006. Environment- and Age-Dependent Plasticity of Synaptic
566 Complexes in the Mushroom Bodies of Honeybee Queens. *Brain, Behavior and*
567 *Evolution* 68:1–14. DOI: 10.1159/000092309.
568 Groh C., Kelber C., Grübel K., Rössler W. 2014. Density of mushroom body synaptic complexes
569 limits intraspecies brain miniaturization in highly polymorphic leaf-cutting ant workers.
570 *Proceedings of the Royal Society of London B: Biological Sciences* 281:20140432. DOI:
571 10.1098/rspb.2014.0432.
572 Handschuh S., Baeumler N., Schwaha T., Ruthensteiner B. 2013. A correlative approach for
573 combining microCT, light and transmission electron microscopy in a single 3D scenario.
574 *Frontiers in Zoology* 10:44. DOI: 10.1186/1742-9994-10-44.
575 Hanström B. 1926. Untersuchungen über die relative Grösse der Gehirnzentren verschiedener
576 Arthropoden unter Berücksichtigung der Lebensweise. *Zeitschrift fur Mikroskopisch-*
577 *Anatomische Forschung* 7:135–190.
578 Harzsch S., Anger K., Dawirs RR. 1997. Immunocytochemical detection of acetylated alpha-
579 tubulin and *Drosophila* synapsin in the embryonic crustacean nervous system. *The*
580 *International Journal of Developmental Biology* 41:477–484.
581 Harzsch S., Hansson BS. 2008. Brain architecture in the terrestrial hermit crab *Coenobita*
582 *clypeatus* (Anomura, Coenobitidae), a crustacean with a good aerial sense of smell. *BMC*
583 *Neuroscience* 9:58. DOI: 10.1186/1471-2202-9-58.
584 Harzsch S., Krieger J., Faulkes Z. 2015. “Crustacea”: Decapoda – Astacida. In: Wanninger A ed.
585 *Evolutionary Developmental Biology of Invertebrates 4*. Springer Vienna, 101–151. DOI:
586 10.1007/978-3-7091-1853-5_4.

587 Harzsch S., Miller J., Benton JL., Beltz BS. 1999. From embryo to adult: persistent neurogenesis
588 and apoptotic cell death shape the lobster deutocerebrum. *Journal of Neuroscience*
589 19:3472–3485.
590 Healy SD., Rowe C. 2013. Costs and benefits of evolving a larger brain: doubts over the
591 evidence that large brains lead to better cognition. *Animal Behaviour* 86:e1–e3. DOI:
592 10.1016/j.anbehav.2013.05.017.
593 Helluy SM., Ruchhoeft ML., Beltz BS. 1995. Development of the olfactory and accessory lobes
594 in the american lobster: An allometric analysis and its implications for the deutocerebral
595 structure of decapods. *The Journal of Comparative Neurology* 357:433–445. DOI:
596 10.1002/cne.903570308.
597 Henne S., Friedrich F., Hammel JU., Sombke A., Schmidt-Rhaesa A. 2016. Reconstructing the
598 anterior part of the nervous system of Gordius aquaticus (Nematomorpha, cycloneuralia)
599 by a multimethodological approach. *Journal of Morphology* 278:106–118. DOI:
600 10.1002/jmor.20623.
601 Herberholz J., Mims CJ., Zhang X., Hu X., Edwards DH. 2004. Anatomy of a live invertebrate
602 revealed by manganese-enhanced Magnetic Resonance Imaging. *Journal of Experimental*
603 *Biology* 207:4543–4550. DOI: 10.1242/jeb.01328.
604 Holst S., Michalik P., Noske M., Krieger J., Sötje I. 2016. Potential of X-ray micro-computed
605 tomography for soft-bodied and gelatinous cnidarians with special emphasis on
606 scyphozoan and cubozoan statoliths. *Journal of Plankton Research* 38:1225–1242. DOI:
607 10.1093/plankt/fbw054.

608 Kenning M., Harzsch S. 2013. Brain anatomy of the marine isopod *Saduria entomon* Linnaeus,
609 1758 (Valvifera, Isopoda) with special emphasis on the olfactory pathway. *Frontiers in*
610 *Neuroanatomy* 7:1–14. DOI: 10.3389/fnana.2013.00032.
611 Köhnk S., Baudewig J., Brandis D., Boretius S. 2017. What's in this crab? MRI providing high-
612 resolution three-dimensional insights into recent finds and historical collections of
613 Brachyura. *Zoology* 121:1–9. DOI: 10.1016/j.zool.2016.11.004.
614 Krieger J., Braun P., Rivera NT., Schubart CD., Müller CHG., Harzsch S. 2015. Comparative
615 analyses of olfactory systems in terrestrial crabs (Brachyura): evidence for aerial
616 olfaction? *PeerJ* 3:e1433. DOI: 10.7717/peerj.1433.
617 Krieger J., Sombke A., Seefluth F., Kenning M., Hansson BS., Harzsch S. 2012. Comparative
618 brain architecture of the European shore crab *Carcinus maenas* (Brachyura) and the
619 common hermit crab *Pagurus bernhardus* (Anomura) with notes on other marine hermit
620 crabs. *Cell and Tissue Research* 348:47–69. DOI: 10.1007/s00441-012-1353-4.
621 Lang G. 2013. Fixierung. In: *Histotechnik*. Springer Vienna, 47–77. DOI: 10.1007/978-3-7091-
622 1190-1_5.
623 Loesel R., Wolf H., Kenning M., Harzsch S., Sombke A. 2013. Architectural principles and
624 evolution of the arthropod central nervous system. In: Minelli A, Boxshall G, Fusco G
625 eds. *Arthropod Biology and Evolution*. Berlin Heidelberg: Springer, 299–342.
626 Macagno ER., Lopresti V., Levinthal C. 1973. Structure and Development of Neuronal
627 Connections in Isogenic Organisms: Variations and Similarities in the Optic System of
628 Daphnia magna. *Proceedings of the National Academy of Sciences of the United States of*
629 *America* 70:57–61. DOI: 10.1073/pnas.70.1.57.

630 Martin P., Dorn NJ., Kawai T., van der Heiden C., Scholtz G. 2010. The enigmatic Marmorkrebs
631 (marbled crayfish) is the parthenogenetic form of Procambarus fallax (Hagen, 1870).
632 *Contributions to Zoology* 79.
633 Meth R., Wittfoth C., Harzsch S. 2017. Brain architecture of the Pacific White Shrimp Penaeus
634 vannamei Boone, 1931 (Malacostraca, Dendrobranchiata): correspondence of brain
635 structure and sensory input? *Cell and Tissue Research*:1–17. DOI: 10.1007/s00441-017-
636 2607-y.
637 Metscher BD. 2009. MicroCT for comparative morphology: simple staining methods allow high-
638 contrast 3D imaging of diverse non-mineralized animal tissues. *BMC Physiology* 9:11.
639 DOI: 10.1186/1472-6793-9-11.
640 Michalik P., Piacentini L., Lipke E., Ramirez M. 2013. The enigmatic Otway odd-clawed spider
641 (Progradungula otwayensis Milledge, 1997, Gradungulidae, Araneae): Natural history,
642 first description of the female and micro-computed tomography of the male palpal organ.
643 *ZooKeys* 335:101–112. DOI: 10.3897/zookeys.335.6030.
644 Mitchell KJ. 2007. The Genetics of Brain Wiring: From Molecule to Mind. *PLOS Biology*
645 5:e113. DOI: 10.1371/journal.pbio.0050113.
646 Mizutani R., Suzuki Y. 2012. X-ray microtomography in biology. *Micron* 43:104–115. DOI:
647 10.1016/j.micron.2011.10.002.
648 Ott SR. 2008. Confocal microscopy in large insect brains: Zinc–formaldehyde fixation improves
649 synapsin immunostaining and preservation of morphology in whole-mounts. *Journal of*
650 *Neuroscience Methods* 172:220–230. DOI: 10.1016/j.jneumeth.2008.04.031.

651 Ott SR., Elphick MR. 2003. New Techniques for Whole-mount NADPH-diaphorase
652 Histochemistry Demonstrated in Insect Ganglia. *Journal of Histochemistry &*
653 *Cytochemistry* 51:523–532. DOI: 10.1177/002215540305100414.
654 Platt KA., Oliver MJ., Thomson WW. 1997. Importance of the Fixative for Reliable
655 Ultrastructural Preservation of Poikilohydric Plant Tissues. Observations on Dry,
656 Partially, and Fully Hydrated Tissues of *Selaginella lepidophylla*. *Annals of Botany*
657 80:599–610. DOI: 10.1006/anbo.1997.0476.
658 Rasmussen KE. 1974. Fixation in aldehydes a study on the influence of the fixative, buffer, and
659 osmolarity upon the fixation of the rat retina. *Journal of Ultrastructure Research* 46:87–
660 102. DOI: 10.1016/S0022-5320(74)80024-9.
661 Richter S., Loesel R., Purschke G., Schmidt-Rhaesa A., Scholtz G., Stach T., Vogt L.,
662 Wanninger A., Brenneis G., Döring C., Faller S., Fritsch M., Grobe P., Heuer CM., Kaul
663 S., Möller OS., Müller CHG., Rieger V., Rothe BH., Stegner MEJ., Harzsch S. 2010.
664 Invertebrate neurophylogeny: suggested terms and definitions for a neuroanatomical
665 glossary. *Frontiers in Zoology* 7:1–49. DOI: 10.1186/1742-9994-7-29.
666 Sandeman DC., Sandeman RE., Derby CD., Schmidt M. 1992. Morphology of the brain of
667 crayfish, crabs, and spiny lobsters: a common nomenclature for homologous structures.
668 *Biological Bulletin* 183:304–326. DOI: 10.2307/1542217.
669 Schmidt M. 2016. Malacostraca. In: Schmidt-Rhaesa A, Harzsch S, Purschke G eds. *Structure &*
670 *Evolution of Invertebrate Nervous Systems*. Oxford: Oxford University Press, 529–582.
671 Snell O. 1891. Die Abhängikeit des Hirngewichtes von dem Körpergewicht und den geistigen
672 Fähigkeiten. *Archiv für Psychiatrie und Nervenkrankheiten* 23:436–446. DOI:
673 10.1007/bf01843462.

674 Sombke A., Lipke E., Michalik P., Uhl G., Harzsch S. 2015. Potential and limitations of X-Ray
675 micro-computed tomography in arthropod neuroanatomy: A methodological and
676 comparative survey. *Journal of Comparative Neurology* 523:1281–1295. DOI:
677 10.1002/cne.23741.
678 Steinhoff POM., Sombke A., Liedtke J., Schneider JM., Harzsch S., Uhl G. 2017. The
679 synganglion of the jumping spider Marpissa muscosa (Arachnida: Salticidae): Insights
680 from histology, immunohistochemistry and microCT analysis. *Arthropod Structure &*
681 *Development* 46:156–170. DOI: 10.1016/j.asd.2016.11.003.
682 Tuchina O., Koczan S., Harzsch S., Rybak J., Wolff G., Strausfeld NJ., Hansson BS. 2015.
683 Central projections of antennular chemosensory and mechanosensory afferents in the
684 brain of the terrestrial hermit crab (*Coenobita clypeatus*; Coenobitidae, Anomura).
685 *Frontiers in Neuroanatomy* 9:1–13. DOI: 10.3389/fnana.2015.00094.
686 Vilpoux K., Sandeman RE., Harzsch S. 2006. Early embryonic development of the central
687 nervous system in the Australian crayfish and the Marbled crayfish (Marmorkrebs).
688 *Development Genes and Evolution* 216:209–223. DOI: 10.1007/s00427-005-0055-2.
689 Vogt G. 2011. Marmorkrebs: Natural crayfish clone as emerging model for various biological
690 disciplines. *Journal of Biosciences* 36:377–382. DOI: 10.1007/s12038-011-9070-9.
691 Ziegler A., Kunth M., Mueller S., Bock C., Pohmann R., Schröder L., Faber C., Giribet G. 2011.
692 Application of magnetic resonance imaging in zoology. *Zoomorphology* 130:227–254.
693 DOI: 10.1007/s00435-011-0138-8.
694

Table 1(on next page)

Average volume of deutocerebral chemosensory lobe (single lobe) of various decapod species.

Taxon	Species	n	DCL volume [mm³] *with optical correction	Reference
Astacida	*Procambarus fallax* cf. *virginalis* (juv.)	7	0.0015	this study (µCT)
Astacida	*Procambarus fallax* cf. *virginalis* (juv.)	7	0.0011/*0.0014	this study (ZnFA)
Astacida	*Procambarus fallax* cf. *virginalis* (juv.)	6	0.0011/*0.0013	this study (Karnofsky)
Astacida	*Procambarus clarkii* (adult)	3	0.0097	Beltz et al. 2003
Homarida	*Homarus americanus* (adult)	2	0.1412	Beltz et al. 2003
Anomala	*Birgus latro* (adult)	1	0.3747	Krieger et al. 2012
Brachyura	*Sesarma* sp. (adult)	3	0.0061	Beltz et al. 2003

1

Figure 1

Volumes of brain compartiments according to the methods applied

Boxplots with median, upper and lower quartiles, minima and maxima, and outliers of volumes of the deutocerebral chemosensory lobes (DCLs) in A, the accessory lobe (AcNs) in B, and the central brain in C. Note that the displayed volumes for DCLs and AcNs refer to the total volumes of both brain hemispheres.

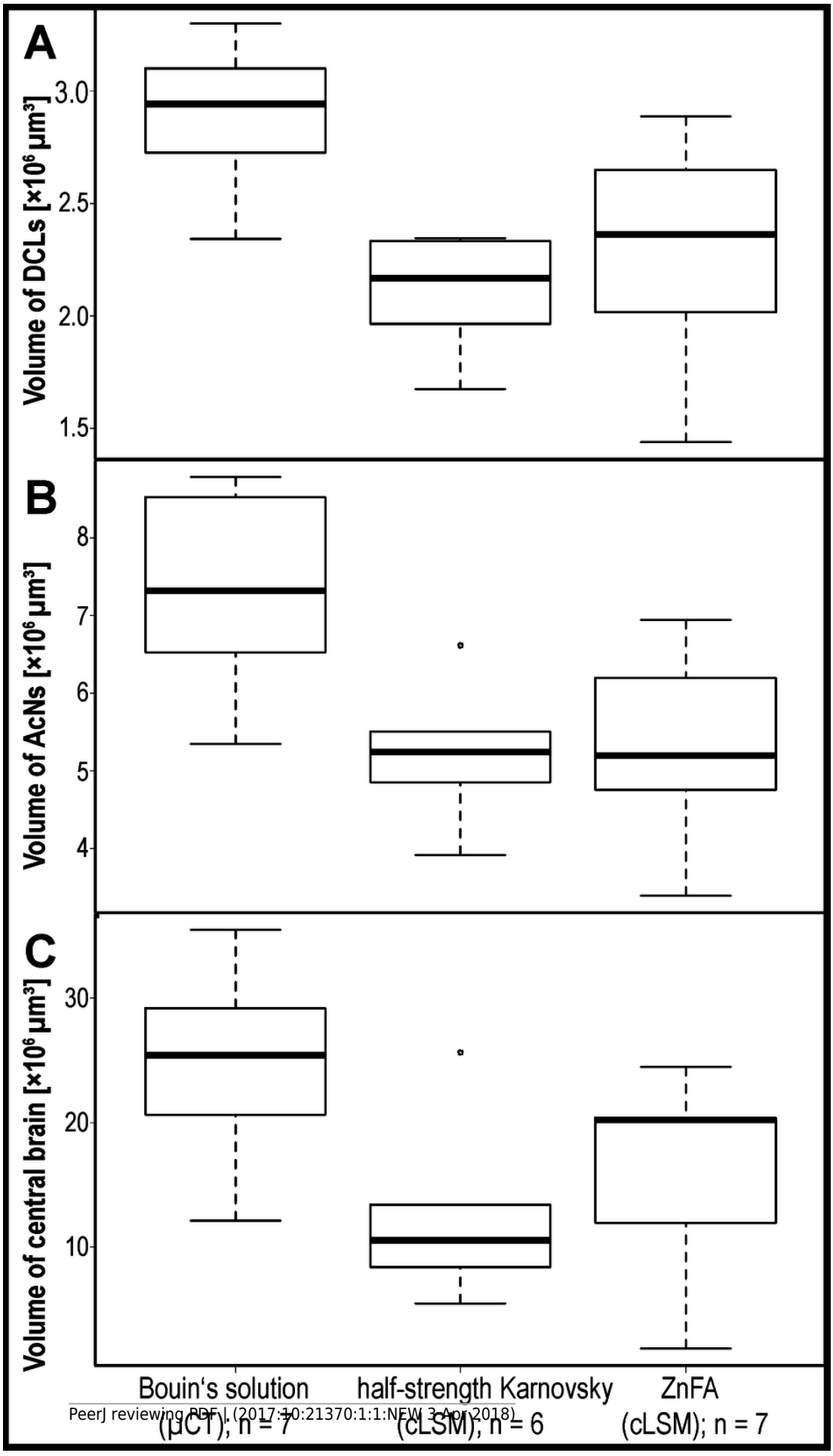
A
Volume of DCLs [×10⁶ µm³]
3.0
2.5
2.0
1.5
B
Volume of AcNs [×10⁶ µm³]
8
7
6
5
4
C
Volume of central brain [×10⁶ µm³]
30
20
10
Bouin's solution
(µCT); n = 7
half-strength Karnovsky
(cLSM); n = 6
ZnFA
(cLSM); n = 7

Figure 2

Comparison of volumetric data based on the methodologic approach of *P. fallax* cf. *virginalis*

Each bar represents the average of reconstructed volumes of deutocerebral chemosensory lobes (DCLs), accessory lobes (ACNs), as well as of the central brain of all specimens analyzed. Note that volumes of the DCLs as well as of the AcNs are plotted pairwise (both brain hemispheres per specimen). Applied methods: µCT (Bouin-fixation), cLSM (half-strength Karnovsky's solution), and cLSM (ZnFA-fixation). The levels of significance between pairs of volumes of brain substructures according to the methods applied are based on Tukey's post-hoc test from a one-way analysis of variance (ANOVA).

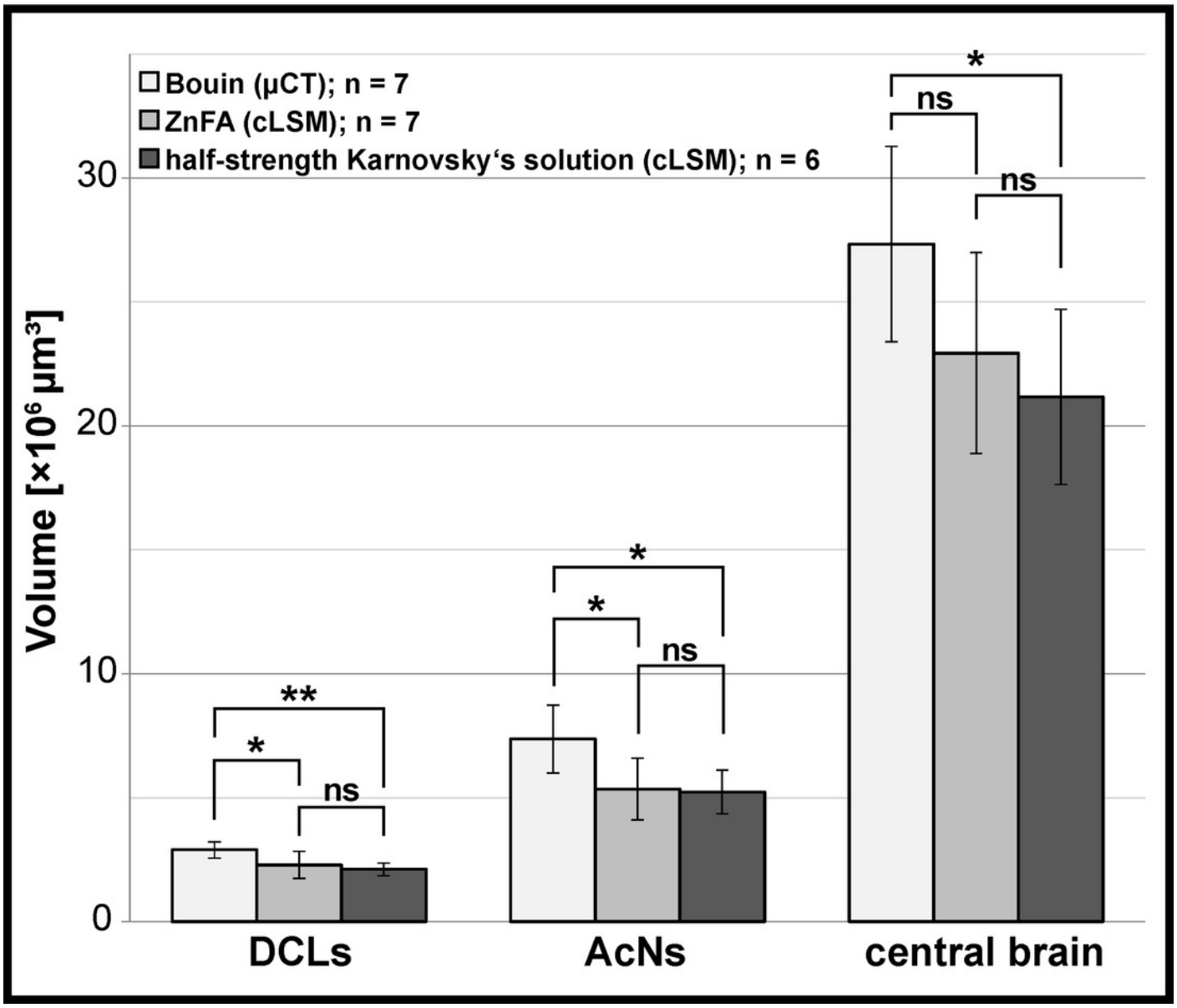
Bouin (µCT); n = 7
ZnFA (cLSM); n = 7
half-strength Karnovsky's solution (cLSM); n = 6
Volume [×10⁶ µm³]
30
20
10
0
**
*
ns
*
*
ns
*
ns
ns
DCLs
AcNs
central brain

Figure 3

Volume renderings of the brain in *P. fallax* cf. *virginalis* from a µCT-scan

The outline of the whole animal body is visualized in A, while in B, a virtual cutaway reveals the position of the brain (white area indicated by a black arrow) from the same perspective. The color-labeled areas in C and D are based on surface reconstruction and show the central brain (orange), the deutocerebral chemosensory lobes (DCLs: green), and the accessory lobes (AcNs: purple). Note that the lateral protocerebrum (latPC) is not reconstructed but visible in dark gray in C and D beneath the ommatidia of the complex-eyes (ce). Other abbreviations: AI, antenna 1 (antennule); AII, antenna 2 (antenna); OC, oesophageal connective.

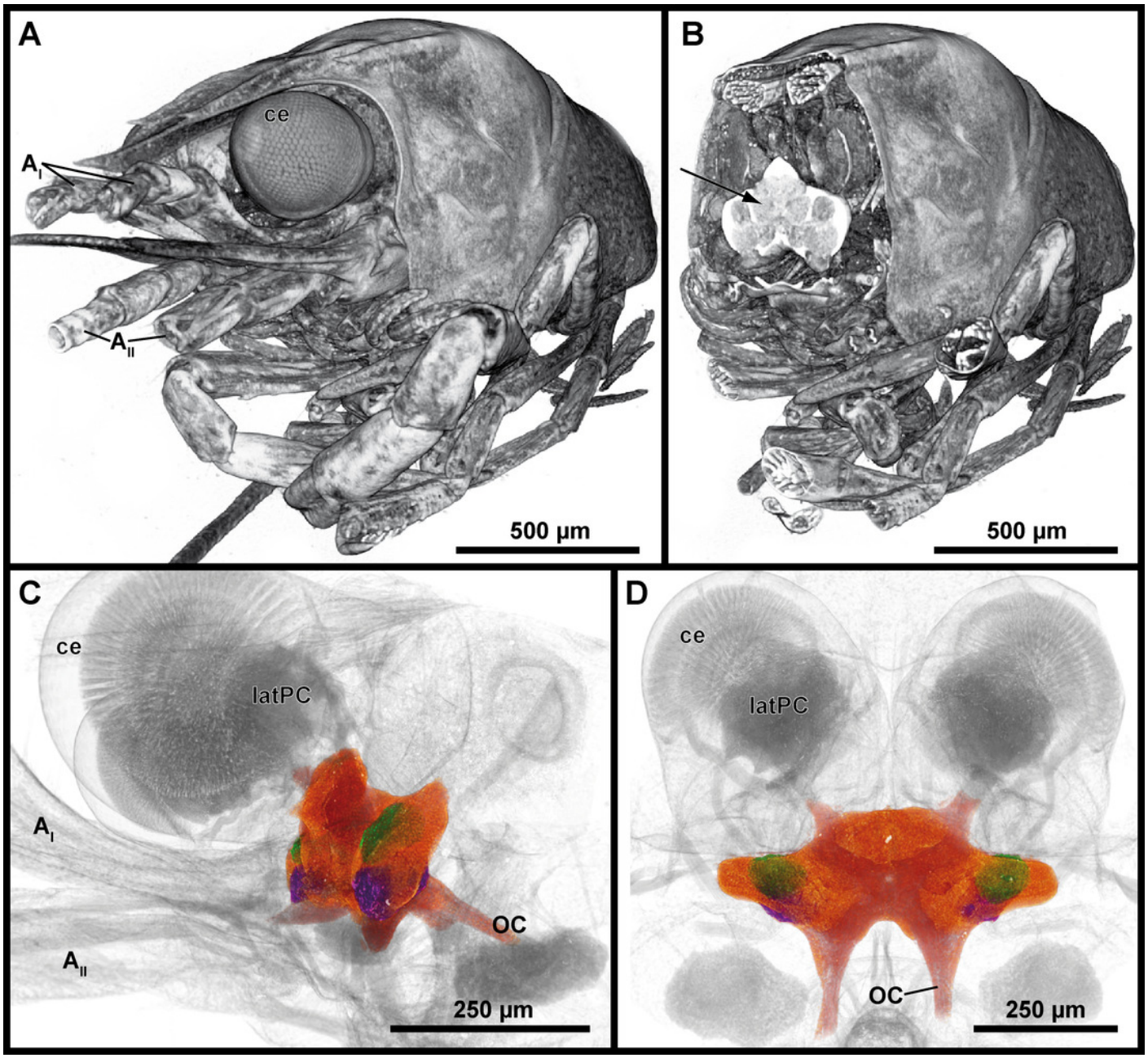
A
ce
A_I
A_{II}
500 µm
B
500 µm
C
ce
latPC
A_I
A_{II}
OC
250 µm
D
ce
latPC
OC
250 µm

Figure 4

Comparison of virtual brain sections of *P. fallax* cf. *virginalis* based on all three methods applied

The scheme in A illustrates the general organization of the central brain (omitting the lateral protocerebrum, nerves, and the oesophageal connectives). Frontal virtual sections of the central brain, according to the tomographic and corresponding fixing method applied, are shown equally scaled in B (µCT using Bouin's solution); in C (cLSM using autofluorescence of half-strength Karnovsky's solution); and in D (cLSM using ZnFA and immunohistochemical labeling against synapsin). Abbreviations: AcN, accessory neuropil; AMPN, anterior medial protocerebral neuropil; AnN, Antenna-II-neuropil; CA, cerebral artery; CB, central body, DCL, deutocerebral chemosensory lobe (olfactory lobe); LAN, lateral antenna-I-neuropil; MAN, median antenna-I-neuropil; PB, protocerebral bridge; PMPN, posterior medial protocerebral neuropil; PNT, projection neuron tract; TN, tegumentary neuropil; 6, 9/11, and 10 indicate somata clusters (6), (9/11), and (10); asterisk indicates olfactory glomeruli in A, C, and D.

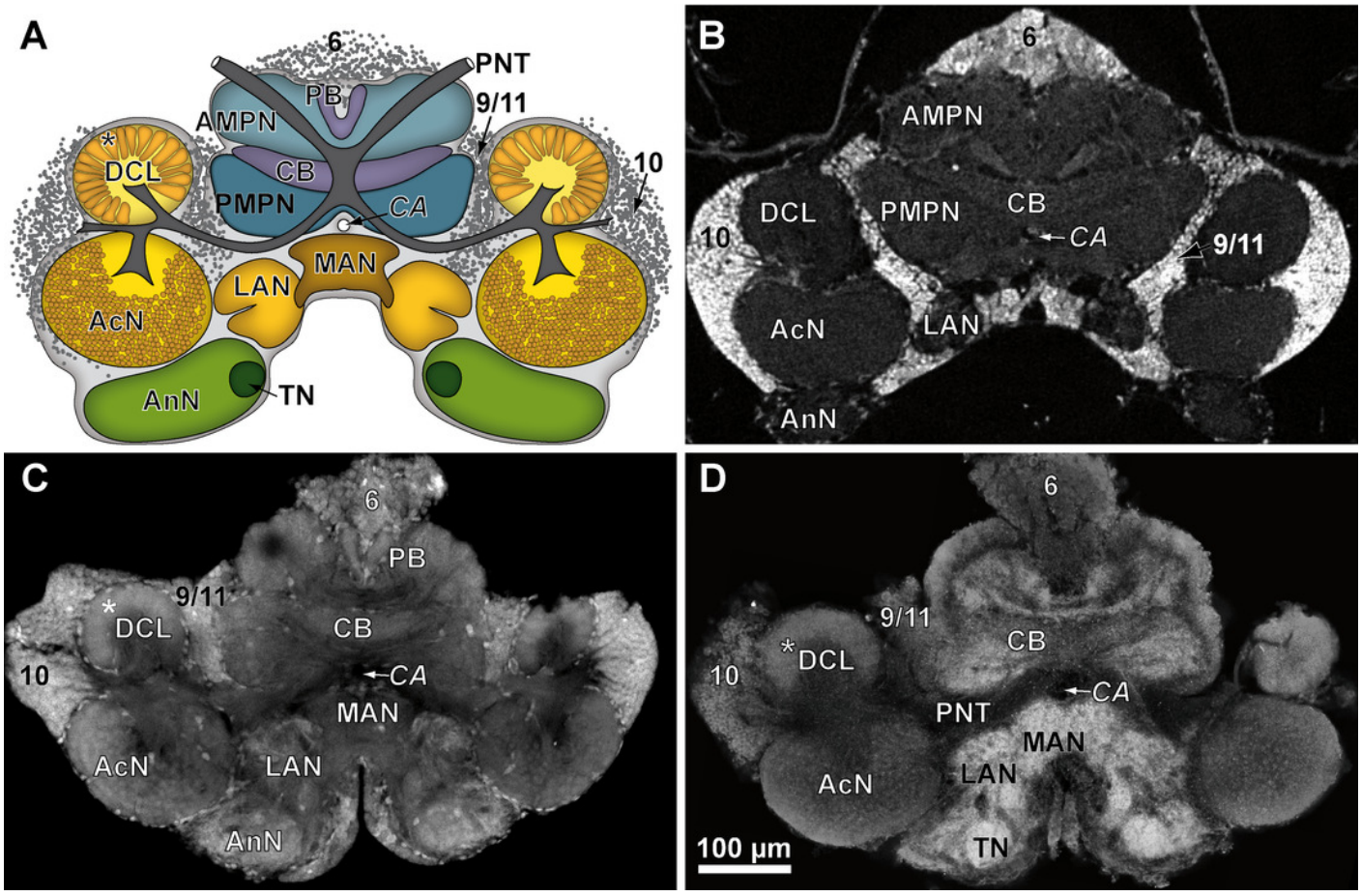
A
6
PNT
PB
9/11
AMPN
*
DCL
CB
10
PMPN
CA
MAN
LAN
AcN
AnN
TN
B
6
AMPN
DCL
PMPN
CB
10
CA
9/11
AcN
LAN
AnN
C
6
PB
9/11
*
DCL
CB
10
CA
MAN
AcN
LAN
AnN
D
6
9/11
CB
*
DCL
10
CA
PNT
MAN
AcN
LAN
100 µm
TN

Figure 5

Virtual sections of adult individual of *P. fallax* cf. *virginalis* and volumes of central brains after different preparation stages

(A) Boxplots with median, upper, and lower quartiles, minima and maxima, and outliers of volumes of the central brain after different stages of preparation for µCT wet-scanning. (B) Frontal virtual slices of the central brain of an adult individual of *P. fallax* cf. *virginalis*. Stage 1) The brains are just dissected and immediately scanned in tap water. Stage 2) Brains are fixed in Bouin's solution. Stage 3) Gradual dehydration and contrast enhancement with iodine (2%) *: Significant difference between stage 1 and 2,3 (Wilcoxon signed rank test: $p = 0.0313$; $n = 6$) ns: No significant difference between stage 2 and 3 (Wilcoxon signed rank test: $p = 0.6875$; $n = 6$)

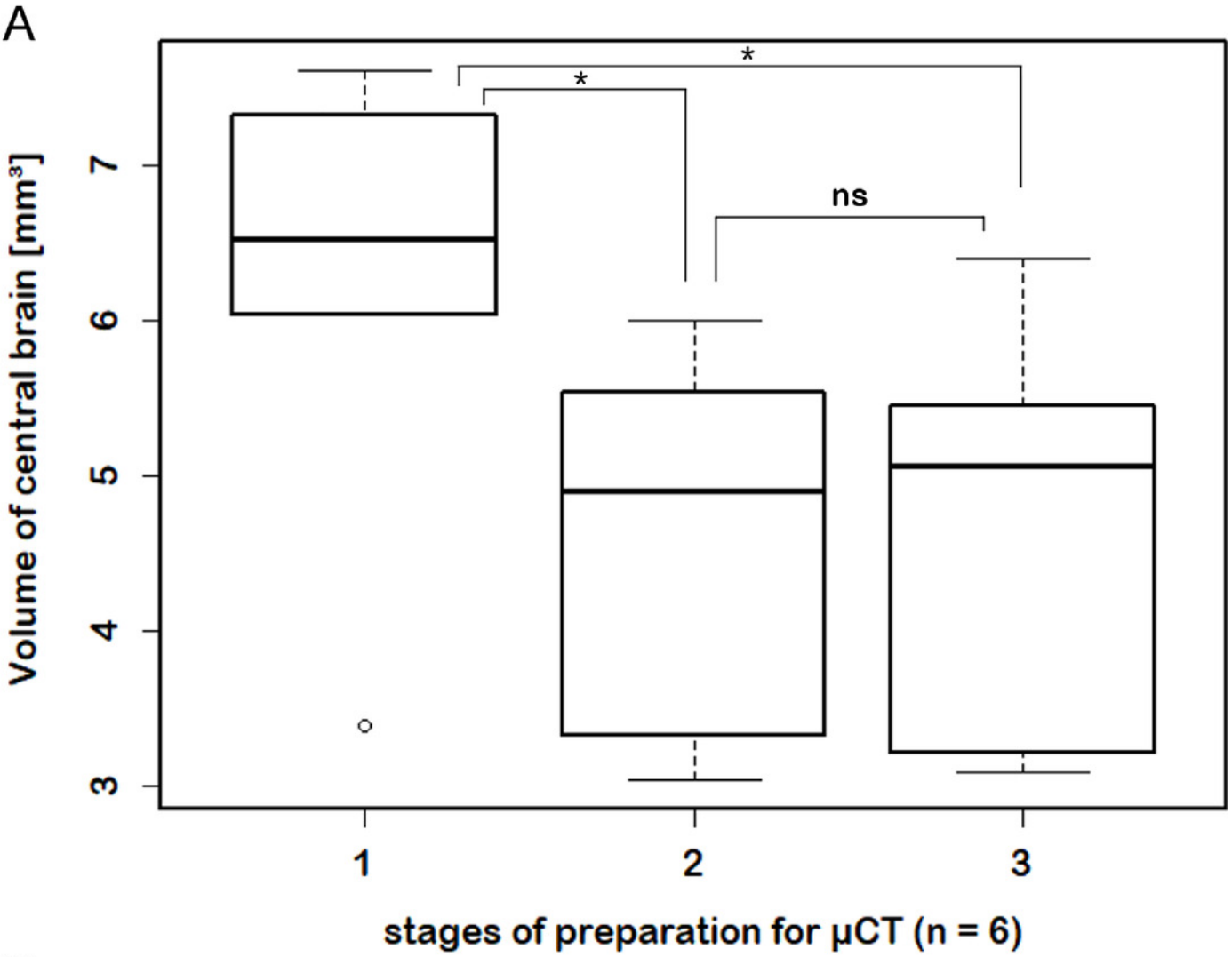
A
*
*
ns
Volume of central brain [mm³]
3
4
5
6
7
1
2
3
stages of preparation for µCT (n = 6)

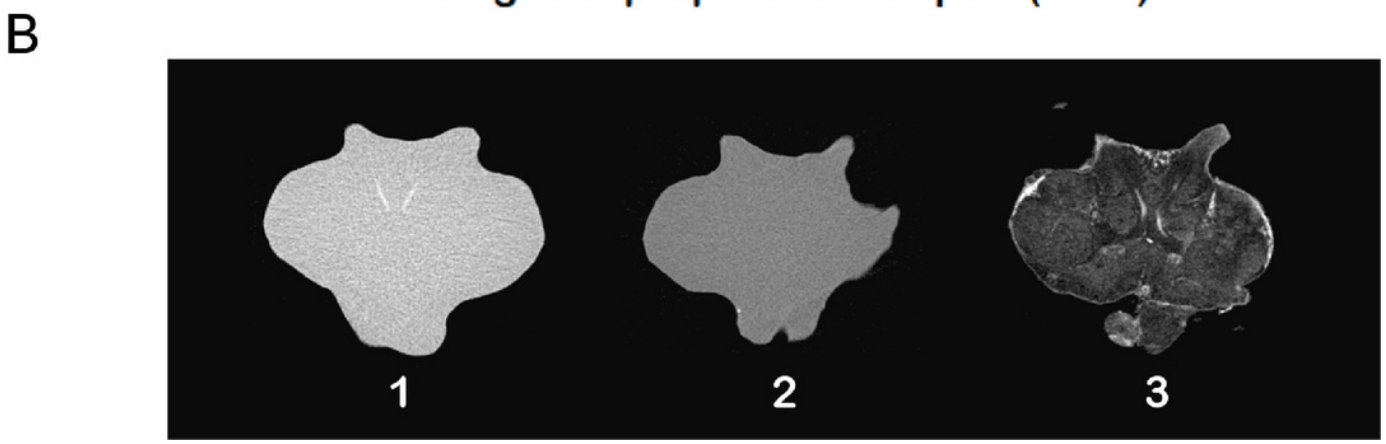
B
1
2
3

Figure 6

Comparison of grayscale-based surface reconstructions of the central brain of two individuals of *P. fallax* cf. *virginalis*

The isosurfaces are based on confocal laser-scanning microscopy of dissected brains fixed in half-strength Karnovsky's solution (A-C) and in ZnFA (D-F), and are shown from different perspectives (A and D: from anterioventral; B and E: from posteriodorsal; C and F: from ventrolateral). Abbreviations: AIINv, antenna 2-nerve; AcN, accessory neuropil; AnN, antenna 2-neuropil; DCL, deutocerebral chemosensory lobe (olfactory lobe); LAN, lateral antenna 1-neuropil; mPC, median protocerebrum; OC, oesophageal connective.

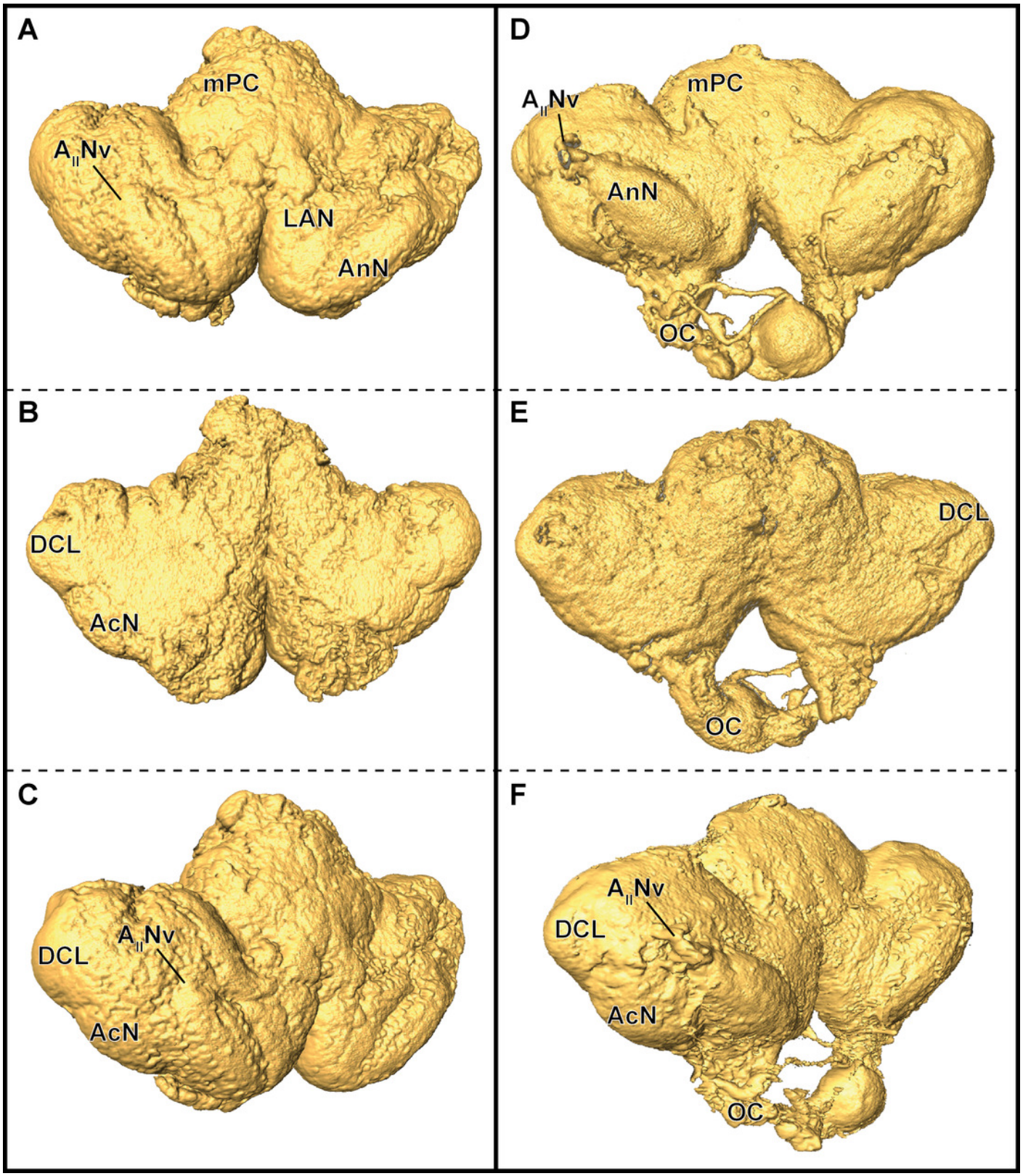
A
mPC
A II Nv
LAN
AnN
D
A II Nv
mPC
AnN
OC
B
DCL
AcN
E
DCL
OC
C
DCL
A II Nv
AcN
F
A II Nv
DCL
AcN
OC